Shear characterisation of pultruded superstructural FRP-concrete push-outs

Etim, O. O., Gand, A., Saidani, M., Fom, P. & Ganjian, E.

Original citation & hyperlink:
Etim, OO, Gand, A, Saidani, M, Fom, P & Ganjian, E 2020, 'Shear characterisation of pultruded superstructural FRP-concrete push-outs' Structures, vol. 23, pp. 254-266. https://dx.doi.org/10.1016/j.istruc.2019.10.004

DOI 10.1016/j.istruc.2019.10.004
ESSN 2352-0124

Publisher: Elsevier

Shear Characterisation of Pultruded Superstructural FRP-Concrete Push-Outs

Offiong Etim, Alfred Kofi Gand*, Messaoud Saidani, Pam Fom, Eshmaiel Ganjian and Eta Okon

School of Energy, Construction and Environment,
Coventry University, Coventry CV1 5FB, UK

*Corresponding author: Email: a.gand@coventry.ac.uk (A. K. Gand)

ABSTRACT

In this paper, an investigation aimed at characterising the behaviour of headed shear studs in push-out testing is presented. The study aims to contribute to the limited knowledge of GFRP-concrete composites, highlighting the predominant failure mode and the underlying variables relevant for predictive analytical equations. Two phases of experimental push-out tests were carried out on composite slabs comprising of normal density concrete (NWC) and glass fibre reinforced polymer (GFRP) connected using steel headed studs. Phase one focused on studying the effects of headed shear stud configuration on the load capacity of the composite slabs, adopting 19 mm diameter studs. Phase two of the study was aimed at characterising the behaviour of the composite slab by varying the headed stud diameters. Two push-out test specimens adopted 12 mm diameter studs, and a third specimen within this phase adopted the 16 mm stud diameter. The dominant failure mode was bearing, net tension and shear out failures of the FRP plates. These modes of failure were distinctly different from those prevalent in the conventional steel-concrete composite, which is either stud shank failure or concrete pull out. The test investigation suggested a successive increase in shear capacity with increased stud sizes. Specimen with stud size of 16 mm attained higher shear strength per stud, approximately 29.4% in comparison to those with 12 mm diameter studs. The study observed that GFRP-concrete composites can mobilize between 40-50 % shear resistances to that of their steel-concrete counterpart's. However, the intensity of bearing failure increases with increase in stud size, thereby compromising the ductility of shear connection.

KEYWORDS FRP, Concrete composites, FRP-concrete, Hybrid system, Shear connectors, Push-out, Stud connections

1 Introduction

The push-out experimental testing is a method of investigating the shear behaviour of a composite connection. BS EN 1994-1: 2004 [1] recommends the push-out experimental testing as a method of investigating the behaviour of shear connection for a composite connection, which is not defined according to established guidelines. The test is aimed at providing information on the properties of the shear connection as will be required for design; therefore, the relevance of the test cannot be overemphasised. Even though the experimental design of the push-out was modelled to assess the performance of stud shear connectors, findings have proven the effectiveness of the test on the use of alternative materials, such as GFRP, modified concrete and hybrid connectors [2, 3, 4]. Researchers have adopted the push-out test for investigations on modifications of steel-concrete connections, including novel and modified shear connectors. Jin di [5] investigating the performance of perfobond connectors in steel-concrete joints reported significant performance of connectors under experimental testing for improved shearing capacity. Yang [6] investigated the performance of various types of demountable stud connectors and reported that failure modes of demountable studs were slightly different from their welded counterpart. The study also reported that the clearance between stud holes and stud shanks had a significant effect on the shear stiffness of stud connectors. Emad *et al*. [7] carried out an experimental investigation on the shear opening of steel beam for slim-floor systems and defined an effective spacing for various shapes of openings to attain maximum shear strength. The investigation adopted the push-out experimental set-up for evaluation of performance, and reliable data analysis was derived from this test method.

Investigations on the influence of concrete modifications have also been known to have a significant impact on the shear capacity of steel-concrete composites under push-out experimental testing. An and Cederwall [8] reported that concrete compressive strength significantly affects the strength of stud connections and suggested that there was a need for the development of a substantial analytical design formula which will account for the interaction between studs and their surrounding concrete area. Ollgaard *et al.* [9] had earlier substantiated the findings from An and Cederwall [8] on concrete compressive strength adding the influence of modulus of elasticity as a combined concrete property which influences the shear capacity of shear studs in lightweight and normal weight concrete. Recent investigations on steel-concrete composite by Kim et al., [10] emphasised that concrete strength not only influences shear behaviour but the stud aspect ratio contributes to the ultimate shear strength and stiffness of the connections.

The reliability of results from push-out experimental testing has been met with a progressive acceptance, to improve test conditions and idealisations in order to capture the comparative behaviour of the ideal structure accurately. Many researchers have reported some of the omitted test conditions that have affected the reliability of results, [9, 11, 12]. Hicks [11] observed a significant difference in results obtained from companion push-out test and composite beam test. His investigations suggested that the observed difference in results were due to the absence of the compression force at the concrete-flange interface exerted by floor loading. Odenbreit and Nellinger [12] observed that the magnitude of the tension force is affected by frictional forces developing at the base of the slab at the interface between the test slabs and the strong floor. Odenbreit and Nellinger [12] reported that the influence of frictional forces causes sliding bearings, which may underestimate the real shear resistance of the connection. However, all these investigations have not refrained or undermined the growing dependence on push-out test experiments for the investigation of novel composite materials including timber-concrete, timber-steel, and most recently FRP-concrete composites respectively. The need for experimental testing to be carried out on novel composites remain a founding basis for the reliance on push-out test experimentation and therefore forms the basis of the method employed to investigate the performance of a novel composite connection between pultruded fibre reinforced polymer and concrete.

Despite the above highlighted research investigations on steel-concrete alternatives and modifications, there have been almost non-existent research investigations on steel alternatives for concrete composite floor and beam systems. However, Fibre reinforced polymers (FRP) have recently witnessed a growing demand for its application in the construction industry as potential replacements for steel materials. The structural potential of FRP is credited to its sustainable benefits over steel in areas of corrosion resistance, fire retardance, relatively high strength-to-weight ratio and low life-cycle maintenance cost. Gai *et al.*, [13] reported essential robustness in a connection of FRP-concrete using

transverse GFRP dowels to prevent sudden brittle failure modes in the connection. Nguyen *et al*. [15] in the research study on push-out investigations for shear connections between ultra-high performing fibre reinforced concrete (UHPFRC) slabs and FRP observed that adequate height and stiffness of stud governed the failure mode and shear performance of the composite connection. Therefore, the author adopted the effective depth-to-stud diameter ratio, h_{ef}/d as a descriptive criterion to evaluate the performance of shear connection and the typical failure modes in UHPFRC – FRP composite. The investigation reported bearing failures for small values of h_{ef}/d ratio and stud shear failures for higher values of h_{ef}/d ratios. Correia [16] also performed push-out evaluation test on Glass Fibre Reinforced Polymers (GFRP) and concrete composites using smaller diameter sizes of 8 mm and 10 mm; it was observed that studs of higher sizes typically resulted in higher shear strengths. There is limited knowledge on FRP-concrete composite performance using shear studs. Available literature has also suggested that FRP girder bearing failures may dominate failure modes associated with FRP-concrete composites and therefore, provides a premise to factor the influence of girder properties into the prediction of shear resistances by this connection. It will be beneficial in seeking consistency with scarce research knowledge to provide a basis for establishing design criteria for FRP-concrete composites.

2 Significance of current study and applications

The significance of this study is to promote the use of lightweight GFRP girders as an alternative to steel in the steel-concrete composite industry. The research study aims to establish performance criteria for the use of FRP-concrete in the design of composite beams for lightweight structures. Therefore, it is essential to enrich the research domain on findings concerned with alternative materials used for composite construction and contribute satisfactorily to the development of design guidelines and standards on the use of GFRP composites. In furtherance of this investigation to bridge the gap in limited knowledge on GFRP concrete composites, experimental findings will scrutinise the application of available theoretical principles in determining the adequacy and accuracy of results to modifying existing models or proposing a definitive model for consideration. The study also presents the underlying analytical principles governing steel-concrete composites in comparison to a recently proposed analytical relationship for estimating the shear strength of GFRP-concrete composites by Nguyen et al. [15].

3 Analytical study

In a composite connection consisting of steel girder component, concrete and steel studs, the shear capacity can be easily determined from the provision in [1], which highlights the adoption of the smaller value between Eqs. (1) and (2):

$$P_{RD} = 0.8 f_u \pi d^2/4 \quad (1)$$

or

$$P_{RD} = 0.29\alpha d^2\sqrt{f_{ck}E_{cm}} \quad (2)$$

Eq. (2) is specified for design purposes with the inclusion of a safety factor value of 1.25. The expression does not only represent the shear capacity of the composite but also describes the failure modes of stud fracture and concrete pull-out failures characterising the composite connection with the smallest value being indicative of the dominant failure mode. This provision under design guideline has been confirmed by researchers to be conservative in describing steel-concrete composite connections. However, the case may not be readily applicable to FRP-concrete composites; hence, the relevance of experimental investigations. The experimental investigation on FRP-concrete composites as observed shows stud deformation and FRP bearing failures being most dominant. This mode of failure is also observed by Nguyen [15] and therefore suggest that Eqs. (1) and (2) stated in Eurocode 4 does not conveniently reflect the failure mode nor shear resistance of an FRP-concrete composite connection. Oehler and Johnson [17] had earlier suggested that the shear capacity of a connection was affected by both concrete properties as well as stud properties assuming the steel girder is rigid. He proposed a formula to account for the contributory influence of this property on the shear performance of the connection. The proposed equation provided a relationship between the compressive, elastic, and modulus properties of these components to evaluate the performance outcome. Oehler and Johnson [17] established the expression:

$$P_p = KA(E_c/E_s)^{0.40} {f_{cu}}^{0.35} {f_u}^{0.65} \quad (3)$$

where,

f_{cu} and E_c represents compressive strength and modulus of concrete, respectively.

f_u and E_s represents tensile strength and modulus of steel, respectively.

The parameter, A, represents the cross-sectional area of the stud shank while K is a constant. If the parameters in Eq. (3) relate with the failure behaviour of steel-concrete composites; it may be convenient to suggest the inclusion of FRP compressive strengths and modulus in the determination of the shear resistance for an FRP-concrete composite observing the influence of FRP flange fibres in the failure mode. This observation may have motivated Nguyen [15] to modify Oehler and Johnson's [17] proposed equation to capture FRP properties, as expressed in Eq. (4).

$$\mathrm{P_{R-MOJ}} = A_{SC}f_u(f_c'/F_u)^{0.7}(E_C/E_{SC})^{0.5}\left(\frac{t_f d\sigma_b E_f}{E_{SC}}\right)^{0.15} \quad (4)$$

where,

t_f = thickness of the girder flanges

d = diameter of the stud shear connectors

σ_b = bearing strength of the girder flanges

E_f = equivalent modulus of elasticity of the flanges

E_{SC} = modulus of elasticity of the shear connectors.

The term $\left(\frac{t_f d \sigma_b E_f}{E_{SC}}\right)^{0.15}$ is empirically determined and represents the influence of the FRP girder to the shear resistance of the FRP-concrete composite connection. Nguyen [15] adopted an ultra- high-performance-fibre-reinforced-concrete (UHPFRC) with far higher compressive strengths and modulus to the conventional lightweight and normal density concrete used by Oehler and Johnson [17]. However, Eq. (4) does not suggest a specific dominant failure as in the case of Eqs. (1) and (2) but only takes account of the active properties of all composite components. Recent studies on PFRP connections have suggested that pin bearing strength of PFRP materials may be crucial in determining the mode of failures associated with bolted connections. This is due to the fibre discontinuities created by the clearance hole on the PFRP material such that, there is increased stress concentration around the clearance holes during loading. There is a need for any proposed analytical equation to signify the expected failure modes as with most composite connections. The purpose of the equations presented above is to illustrate the challenge in formulating an effective analytical equation for predicting shear strength in PFRP-concrete composites. This challenge serves as further motivation for the current experimental investigation presented in this paper. The current test is designed under the guidance for push-out test specified in Eurocode 4 [1] for steel-concrete composites. The experimental setup and test procedure are described in subsequent sections of this paper.

4 Methodology

The tests were carried out in two phases, I and II. An investigation carried out in Phase I focused on bolt configuration using a constant stud size and embedment depth. Phase II investigation only varied the stud size diameter with constant depth and bolt configuration. Experimental studies involving push-out test methods typically require the setting up of a test rig under which the performance of specimens will be evaluated. The test rig setup is carefully designed to minimise errors, which may result from loading or specimen instability. Therefore, experimental components are conveniently positioned to check for resultant outcomes. Relevant details on the material property were obtained earlier from the characterisation of composite materials and are provided in subsequent sections for informative and interpretive purposes in an attempt to simplify the behavioural analysis as detailed in this research.

4.1 Mould fabrication

Figure 1 shows a bespoke steel mould prefabricated using 6 mm steel plates. The mould has one side open to accommodate a timber board with the flexibility to adjust the thickness of the composite slab thickness up to 200 mm. The timber board provides support for the shear headed stud through perforated holes, which facilitate the positioning of the headed stud for varying arrangements. The headed stud embeds into the concrete by 100 mm. The mould can support geometric dimensional volume of 500 mm × 550 mm × 150 mm of concrete, adopted for this study. Reinforcement bars were introduced to ensure stability and strength improvement for the concrete. The rebars were cut and formed into rib cages inserted into the mould in preliminary preparation for the concrete curing. The rebars were designed transversely in a rectangular arrangement to fit into the mould and held together by longitudinal bars. The rectangular rib rings acted as confinement rings around the concrete with a concrete cover requirement of 25 mm.

Fig. 1. The bespoke composite slab concrete casting mould.

4.2 Description of materials

Two major materials, namely GFRP and NWC (normal weight concrete) are coupled together with the aid of a demountable steel stud. The concrete slabs were predetermined from a mix design and cured into the bespoke mould to achieve the required geometric shape. The FRP girders were factory fabricated from engineering composites company and cut into 600 mm sizes. The shear studs utilised were hexagonal headed Grade 5 (8.8), high tensile part threaded bolts to BS 1768.

4.2.1 Concrete design and specifications

Normal weight concrete (NWC) design was specified accordingly using the BRE standard method for the design of mix proportions. The trail mixes were corrected to achieve some level of consistency in the mix, and the three different batches of concrete were made for the three pairs of slabs representing the three specimens. Details for the concrete specimen, including the characteristic properties, are outlined in Table 1. Concrete cubes and cylinders were cured similarly as their companion slabs for 21 days (phase I) and 28 days (phase II) and subjected to a compressive strength test using the 2000 kN Avery-Denison machine. The compressive strength is the dominant concrete property required for the stud to mobilise their resistance against shear loads. Hence, the tensile strength of the concrete is not significant in this experimental investigation and therefore omitted.

Table 1.

Concrete cylinder/cube properties.

Specimen ID ⇨	PO-SR-S1	PO-SG-S2	PO-DR-S3	PO-12B-S4	PO-12B-S5	PO-16B-S6
f_{ck}/f_{cu} (MPa)	47.2/49.9	47.2/49.9	47.2/49.9	28.2/46.0	27.8/45.3	25.8/40.0
E_{cm} (GPa)	30.5/31.3	30.5/31.3	30.5/31.3	23.56/30.1	23.4/29.9	22.5/28.1

f_{ck} – concrete cylinder strength, f_{cu} – Concrete cube strength and E_{cm} – Concrete elastic modulus

The concrete curing process was carried out in batches with two concrete slabs per batch. Six concrete slabs with uniform geometric dimensions (500 mm × 550 mm × 150 mm) were cast from three different curing batches using the same mix design. Each concrete slab was cast in the vertical position for ease of embedment of the steel shear studs. The concreting process was carried out in three levels of vibration to ensure suitable concrete quality.

5 Specimen configuration, test setup and instrumentation

The push-out specimen was a composite connection of a pultruded glass fibre reinforced polymer (GFRP) I-beam section 600 mm in height with constant uniform cross-sectional geometry (cross-section 200 mm × 200 mm and average thickness of 10 mm) and two pre-cast concrete slabs of constant cross-sectional geometry (500 mm × 550 mm × 150 mm in width, length and thickness) respectively. A demountable stud connection was used to ensure the composite action between the two materials. Following the parametric analysis geared towards the evaluation of shear performance for the composite connection, the variability of the composite configuration was necessary to obtain a robust study. This resulted in the segmentation of experimental activities within the phases.

5.1 Phase I test specimens

This phase focused on the stud configuration as provided in standard codes. Therefore, the specimen labelling reflected more of the configuration when compared to the specimen labelling in phase 2, which centred on stud diameter. Three specimens were designed as follows; 2no. bolts per row for a single-row, 2no. bolts per row for a double-row and a staggered bolt configuration of 6no. bolts, respectively. The connection was achieved using a 19mm stud size diameter. The two stud single-row configuration (see Fig. 2a) was modelled after the provisions of BS 5400-5 (2005) and the two stud double-row as specified in [1]. The staggered 6no. bolt configuration was modelled after common practice in construction (See Fig. 2b). The specimens were labelled to reflect the configuration as follows; PO-SR-S1, PO-DR-S2 and PO-SG-S3. The notation PO represent Pushout; SR, DR, SG represent single-row, double-row and staggered configurations, respectively; and S1 represent test specimen 1, 2 or 3. The concrete mix design for this phase was from a single batch and cured for 21 days.

5.2 Phase II test specimens

Specimen details were of constant configuration (constant embedment depth, stud spacing and loading process) and analogous to that specified in the annexe of [1] for push-out test configuration requirements as presented in Fig. 2c. Three specimens were developed for the test and the stud size adopted for composite connection varied as follows; two of the specimens used 12 mm stud size diameter and the third specimen used 16 mm stud size diameter respectively. Strain gauges were secured to the shear studs and FRP flanges to determine the strain on the stud and the perforated stud clearance areas of the FRP flange for comparative analysis. Specimen designation of codes carefully reflected the parameter to be analysed and the size of the stud. PO-12B-S4 can be illustrated as; PO represent push-out, 12B represents 12 mm diameter stud S4 represents specimen number 4. However, one specimen was characterised with the use of 16 mm diameter studs while the other two specimens used 12 mm diameter studs, respectively. PO-12B-S4 had strain gauges attached to each stud closer to the stud cap embedded in concrete. Specimen PO-12B-S5 strain gauges were placed on the FRP plates at 25 mm above the clearance hole of the stud (see Figs. 3c and 4c). Specimen PO-16B-S6 had strain gauge embedment on the studs positioned close to the FRP- concrete interface) and on FRP plates in a similar position to PO-12B-S5, see Fig. 3 (a-c). The concrete slabs were cured for 28 days.

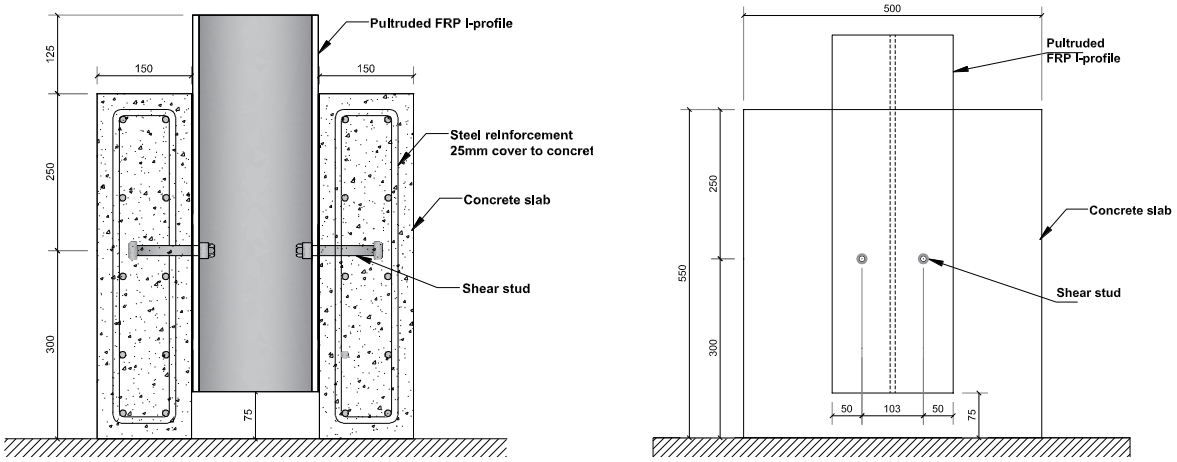

a) Single row stud arrangement (PO-SR-S1)

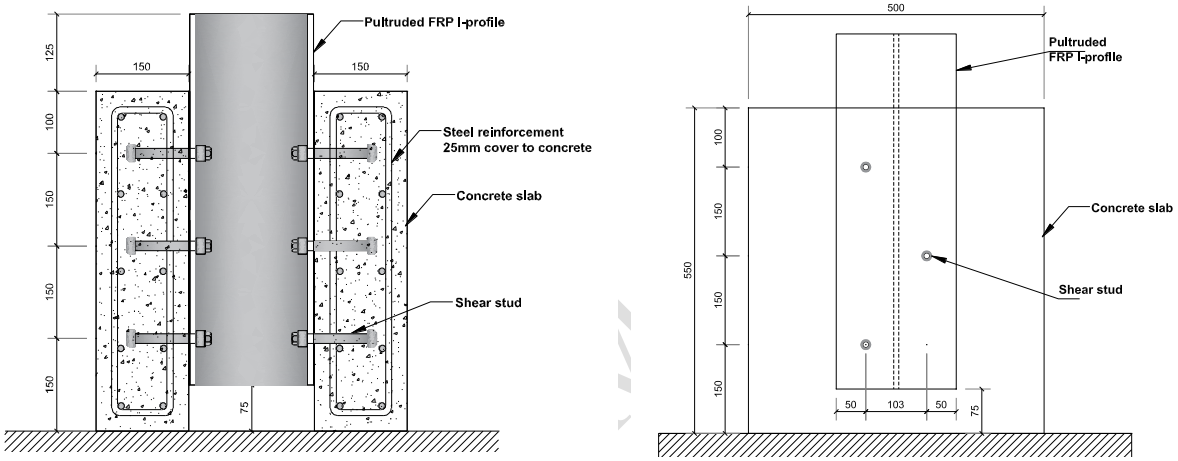

b) Staggered stud arrangement (PO-SG-S2)

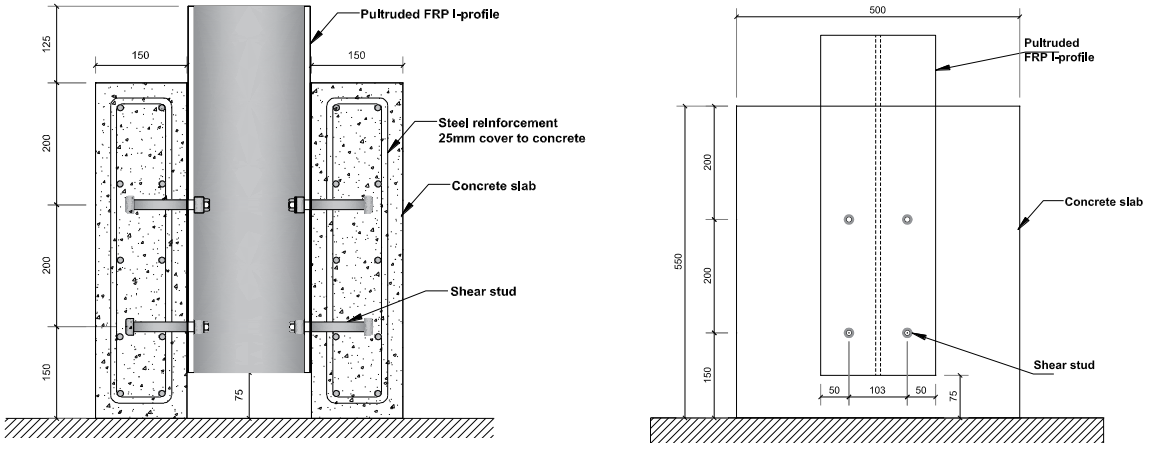

c) Double row stud arrangement (PO-DR-S3)

Fig. 2. Specimen configurations (all dimensions are in mm - not drawn to scale).

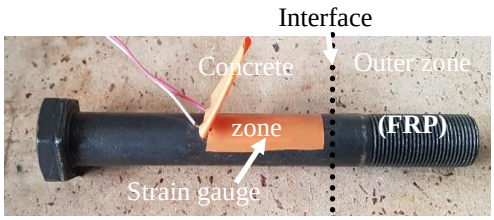

(a) Strain position at FRP-concrete interface

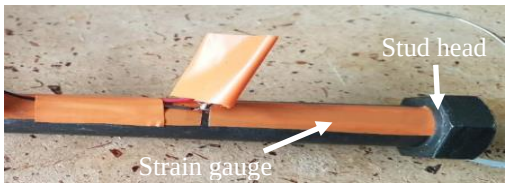

(b) Strain position near shear stud head

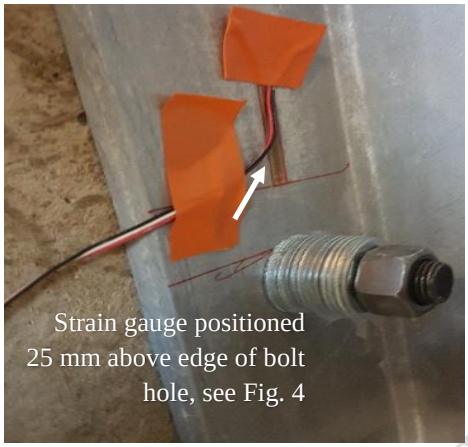

(c) Positioning of strain gauge

Fig. 3. Strain gauge configuration on specimens.

5.3 Test setup and instrumentation

The test rig, as shown in Fig. 4 details the testing mechanism designed to apply substantial loading to a degree capable of deforming the shear studs up unto failure in the composite section. The push-out loading was applied by a 500kN capacity, by a manually operated hydraulic jack. An output setup using a data logger acts as a feedback system to record the intensity of loading and the slip.

To ensure evenness at the base of the slabs for uniform distribution of load, the specimens were placed on a level solid floor and plumbed. A steel plate was positioned at the top of the GFRP section to distribute the load applied to the specimen. Two displacement transducers were placed on opposite sides of the plate to measure the longitudinal slip during loading of the I-section against the reinforced concrete slabs (Fig. 4b). Fig. 3 (a) and (b) illustrate the strain gauge position on the shear stud. Figure 3c shows the strain gauge placed at 25mm above the stud clearance holes on the GFRP flanges. Hydraulic press jack was used in exerting load gradually and progressively at a significantly lower loading rate until failure. The data loggers act as a feedback system to record the intensity of loading and the slip (displacement). Strain gauges are attached to the shear studs and FRP flanges to determine the strain on the stud and the perforated stud clearance areas of the FRP flange for comparative analysis.

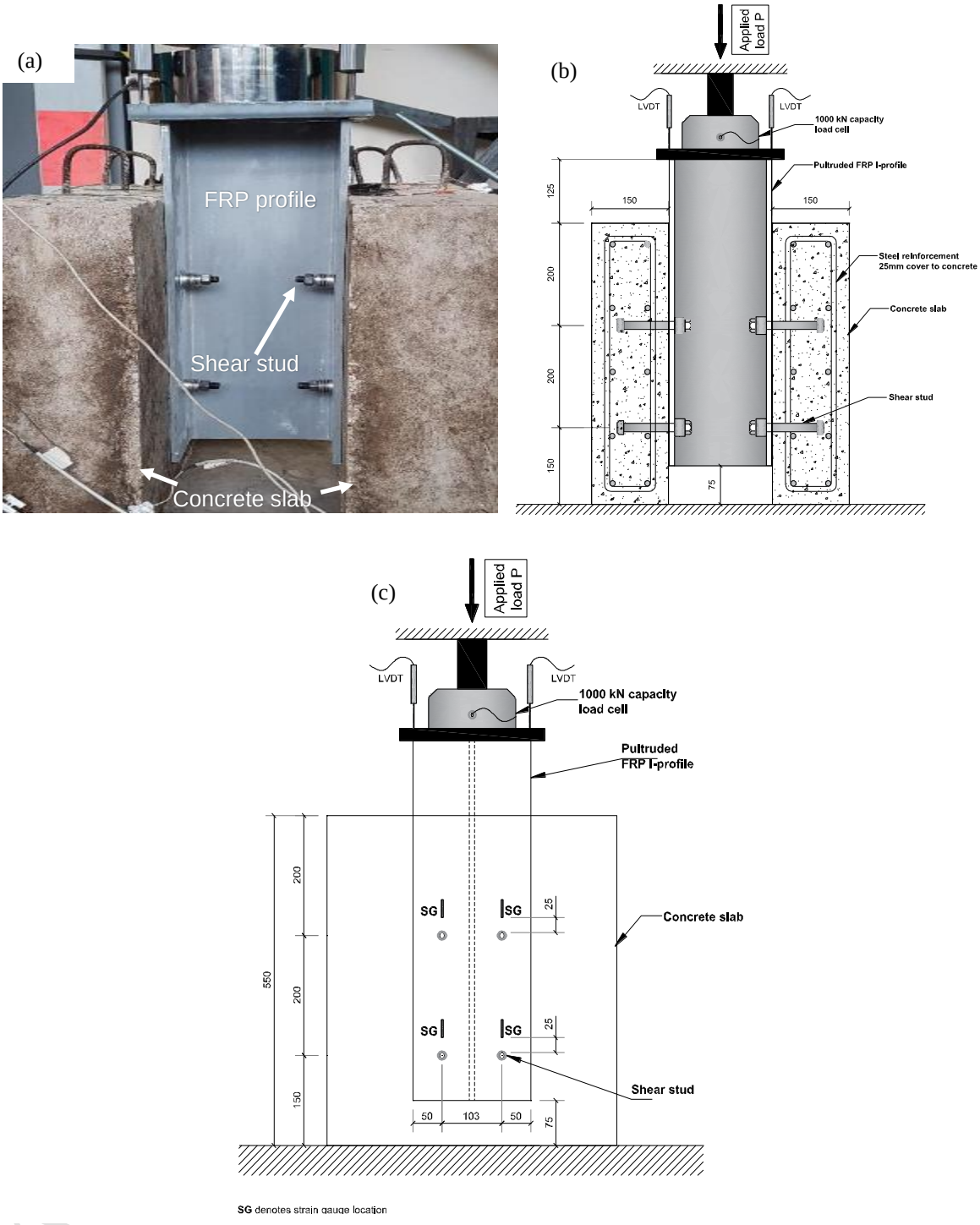

Fig. 4. Test setup - *(a)* experimental arrangement, *(b)* schematic cross-section *(c)* side elevation showing typical strain gauge locations on the FRP profile (all dimensions are in mm - not drawn to scale).

6 Results and discussion

The results obtained from both phases of the experiment involving a total of 6 push-out specimens is reported and analysed to illustrate the implication of the connections comparatively against existing standard guidelines for steel-

concrete composites. The analysis centers on performance evaluation to determine the mode of failure, shear capacity and ductility among a host of criteria for the composite connections. Summary of test results is presented in Table 2.

Table 2.

Summary of test results of push-outs.

Specimen ID (1)	Ultimate load, P_U (kN) (2)	Slip at ult. load, $S_{U,}$ (mm) (3)	Experimental strength per stud $P_{Exp,}$ (kN) (4)	Stiffness of shear connection, K, (kN/mm) (5)	Failure mode (6)
PO-SR-S1	300.5	10.7	75.1	48.3	Bearing failure of FRP flanges/bending of shear stud/severe delamination of FRP flanges
PO-SG-S2	443.7	10.8	74.0	105.2	Bearing failure of FRP flanges/bending of shear stud/severe delamination of FRP flanges
PO-DR-S3	552.6	11.5	69.1	75.5	Bending of flanges/tension/bearing failure (FRP)
PO-12B-S4	333.0	8.0	41.6	62.5	Bearing failure of FRP flanges/bending of shear stud/severe delamination of FRP flanges
PO-12B-S5	385.0	8.9	48.1	96.4	Bearing failure of FRP flanges/bending of shear stud/severe delamination of FRP flanges
PO-16B-S6	431.0	10.9	53.8	110.0	Bearing failure of FRP flanges/bending of shear stud/severe delamination of FRP flanges

6.1 Failure mechanisms of the push-outs

Steel-concrete composites are typically associated with concrete pull-out, sprawling and stud fracture failure, respectively. However, when the component materials are altered, other failure modes can be expected as have been reported in the literature. Nguyen [15] has reported the failure mode observed from research investigations on FRP-concrete as dominantly bearing failure around the holes on the flanges of both HFRP (hybrid fibre reinforced polymer) and GFRP, respectively. The use of 10 mm and 16 mm sizes of various types of steel stud was used alongside the combination with epoxy adhesive for several specimens, but the failure observation was never without the inclusion of bearing failure for the FRP material, which indicated a low compressive strength of the FRP flanges against steel counterpart. This primary observation reemphasises the importance of the push-out experimental testing as highlighted in [1] for the investigation of composite connection consisting of non-typical members (i.e. alternative materials to concrete and steel). Figure 5 illustrates the general failure mode observed in the current study. It corroborates the previous study undertaken by Nguyen [15] on the predominant bearing failures on the FRP flanges. Another vital failure observation was the single curvature bending of the studs as described and reported by Odenbreit and Nellinger [12] for shear studs in solid slabs. However, the single curvature bending was more evident in stud size diameters less than 19

mm diameter stud as shown in Fig 5. A combined shear through and bearing failures were observed on the FRP flanges for stud size diameters of 19 mm. The depth of the shear through failures was higher for larger stud sizes on the FRP. Fibre delamination was severe around the bolt holes. Fibre failure noise highly characterised experimental testing involving fibre materials due to the fibre-matrix relationship depicting stress levels within fibres as well as energy loss from the breakdown of the fibres. Therefore, fibre failure sound was anticipated during the experiment and observed mildly at about 45 – 74 % of ultimate load with louder fibre failure sounds observed between 85 % until failure for all test specimens.

Another predominant failure mode, the shear-out failure occurred on the flange panel of specimen PO-DR-S3, utilising the 19 mm bolt. As outlined earlier, the 19 mm stud hardly deformed and with the double-row configuration (PO-DR-S3), it provided more resistance to the shear load allowing for significant damage to the flange panel. The specimens tested in phase 2 (PO-12B-S4, PO-12B-S5) and PO-16B-S6) proceeded on a simultaneous deformation of shear stud during loading at an almost inconspicuous disparity among stud members. The eventual failure of stud showed that almost all stud members deformed at similar angles with a visually insignificant difference, which may be due to varied differences in concrete strength mobility of non-homogeneity in the concrete mix, as outlined in Table 3. The mean value for the deformation angle was marginally similarly. The variance in the deformation angle becomes more significant with higher stud sizes as seen in the table. In the single curvature bend on studs, it may appear that the bearing of the stud and nuts on the FRP initiated the second type of failure, which dominated the eventual failure of the connection. This type of failure seems to govern the FRP-concrete connection against the conventional stud fracture and concrete pull-out failures typical of steel-concrete composites. The transition from the linear zone of the stud deformation unto the combine nonlinear bending and bearing on the FRP occurred at 78% of the ultimate failure load of 333 kN with a corresponding slip of 3.9 mm for PO-12B-S4. The transition for PO-12B-S5 was at 83% of the ultimate load of 385 kN at a corresponding slip of 3.2 mm. Specimens PO-12B-S4 and PO-12B-S5 showed a similar pattern of failure without any significant variation in behaviour. The shear studs were all bent at similar angles at a simultaneous rate during the test until the initiation of bearing failure on the FRP girder gradually became conspicuous up until ultimate failure, where no further load was reasonable. The longitudinal depth of bearing failure was measured to be approximately 4 - 4.5 mm at single curvature deformation of the studs. The extent of the damage to the flange panel is presented in Fig. 6.

Table 3.

Stud deformation angles.

Stud sizes	Top row deformation (degrees)		Bottom row deformation (degrees)		Mean value (degrees)	Standard deviation
	Left	Right	Left	Right		
12 mm bolts	16.0	17.0	16.5	18.0	16.9	0.74
16 mm bolts	17.0	14.0	17.0	19.0	16.8	1.78

The 16 mm stud diameter specimen of an exact stud arrangement reaffirmed the mechanical behaviour of the composite connection bearing the same stud configuration. The deformation of the stud was observed to be simultaneous and a gradual transition from linear response to the single curvature bending of the 16 mm shear stud unto the bearing failure of the FRP material propagated around the clearance holes. However, unlike the first phase of testing for specimens PO-DR-S3 (utilising 19 mm stud), net tension failures of the FRP plates did not occur. The initiation of bearing failure was observed at approximately 348 kN loading, and ultimate failure was recorded at 430 kN. Specimen PO-DR-S3 recorded an ultimate load of 552.7 kN with a corresponding slip of 11.5 mm. The predominant modes of failure observed on this specimen included a clear tensile tear out of the FRP flanges with the tension line passing right above the bolt holes and extending out to the edge of the FRP on one end, and the web-flange junction on the other end. The failure line followed a straight longitudinal shear line down to the bottom end of the flange. This type of failure has been reported by Mottram [18]. A consistency with phase 1 and reports from [15] will imply the contribution of FRP flange properties in predicting the shear resistance of FRP-concrete composites.

Fig. 5. Failure of specimens and components.

Fig. 6. FRP flange panel failure and extent - specimen PO-SR-S2.

6.2 Load – slip relationships

Load –slip relationships for all specimens are presented in Figs. 7 and 8 for the two phases of testing, respectively.

6.2.1 Phase 1 load-slip plots

Presented in Figure 7a is the load-slip plot for all three specimens tested under phase I. The load versus slip curve for PO-SR-S1 (a single row or four-bolt configuration) showed a reasonably linear behaviour before reaching an ultimate load of 300.5 kN at an average longitudinal slip of 10.71 mm. The curve exhibits a zigzag behaviour from when the load was increased from 128 kN till the failure load and post-failure. From the observation of the concrete slabs after the experiment, there were no visible cracks on either of the slabs that might have been suggestive of the observed irregular profile. However, it was common with all specimens and more suggestive of inner fibre delamination response to loading.

After the ultimate resistance is reached, the curve exhibits a non-linear and gradual drop in resistance up until failure. A pseudo-ductile behaviour is exhibited in the non-elastic zone, mainly as a result of the steel bolts. PO-SG-S2 (staggered or six-bolt configuration) exhibits a similar behavioural response to PO-SR-S1with an initial stiffness at loading up to 25 kN. Redistribution of loading with the shear studs seemed a likely occurrence in this setup as the shear response at yielding was slower before attending its peak at 443.7 kN with a corresponding slip of 11 mm. PO-DR-S3 (double row or eight bolt configuration) provided the highest shear resistance and became the adopted configuration for phase two testing. The ultimate load was obtained at 552.7 kN with a corresponding slip of 11.5 mm. The curve exhibits a more sustained linear zone than the other specimens with corresponding nonlinear zone beyond yielding with a sudden drop in load which might describe the net tension failure reported in Section 6.1.

6.2.2 Phase 2 load-slip plots

Presented in Figure 7b is the load-slip plot for the three specimens investigated under phase II. PO-12B-S5 specimen showed evidence of slip movement at a load of about 33 kN then provided a conspicuous slip at a load of about 88 kN which might have been due to the stud bearing unto the clearance hole. The specimen behaved linearly transitioning at yielding unto a nonlinear behaviour after that up until failure occurred. The specimen recorded an ultimate load of about 380 kN at which time the bearing failure was already initiated on the GFRP and sustained a combined bearing and stud deformation until failure where no further load was admissible. PO-12B-S4 (similar configuration and stud size to PO-12B-S5) also behaved linearly until yielding occurred then behaved nonlinearly until failure occurred. The ultimate load recorded was 13.5% less than PO-12B-S5 at 385 kN. Slip values for PO-12B-S4 and PO-12B-S5 were approximately 8mm and 8.9mm, respectively. The reason for the difference in failure load may be due to a combine non-homogenous weakness in the FRP and a non-consistency in the concrete mix around the stud area for the various specimens. PO-16B-S6 had similar behaviour to the PO-12B-S4 and PO-12B-S5 as all three samples failed in a ductile manner depicting a combined and simultaneous deformation of both stud and bearing failure of the FRP flange. However, the 16 mm stud peaked at a higher load of 430 kN about 10.5% greater than PO-12B-S5. The slip of 10 mm was obtained at the point of yield to avoid the contribution of the FRP flange bearing to ductility forming a pseudo-ductile behaviour in the nonlinear zone. The plot in Fig. 8 represents the load slip curve for both left and right load-displacement-transducers (LVDTs), and it can be seen that the loading was fairly distributed on the specimen as well as the resistance and slip throughout the connection. This is equally evident from the stud deformation and depth of bearing failure captured.

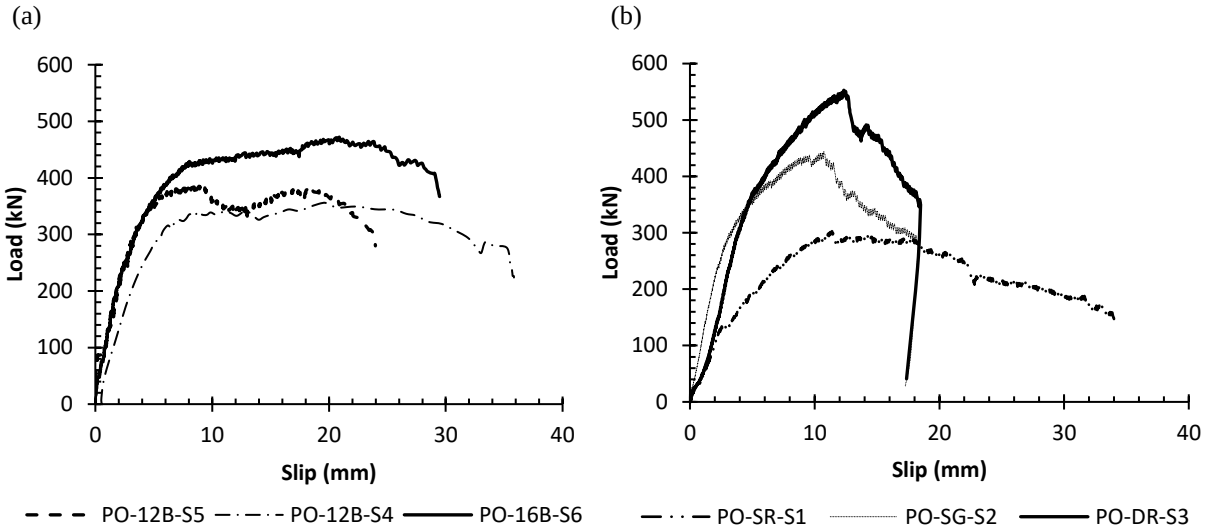

Fig. 7. Load-slip relationship.

6.2.3 Comparison of specimen PO-DR-S3, with 19 mm stud and specimen PO-16B-S6, with 16 mm stud

Presented in Figure 9 is the load-slip relationship of 16mm and 19mm diameter studs for comparative analysis. This comparison highlights the peculiarities between the 16 mm and 19 mm shear studs under the same stud arrangement. The load-slip curve for PO-DR-S3 differs distinctively from PO-16B-S6 due to the sharp fall of the curve at the peak. The sudden drop from the peak represents the intensity of the failure observed in the 19 mm stud size specimen. The subsequent reduction observed on the curve after the sharp drop at the peak represents a fibre deformation due to bearing failure is sustained throughout the connection during experimental testing. The curve for the 19 mm stud (PO-DR-S3) illustrates a failure entirely dominated by bearing failure even though there was an appreciable bending of the stud represented by the nonlinear zone of the curve, but the sudden fall from the peak exhibits the bearing failure as an override to the stud deformation. Specimen PO-16B-S6 with 16 mm studs, on the other hand, produced an extended deformation are relatively constant push out load and illustrating ductility only, in this case, the ductility is made possible by a combined interaction of stud and flange panel failure.

The ductility provided beyond the point of yield is not reliable and cannot be adopted for design as prescribed by [1]. Specimen PO-DR-S3 with 19 mm studs exhibited a higher peak load of 552.7 kN, 22% greater than the specimen with 16mm studs. However, the specimen with 19 mm studs may represent an unsafe upper boundary solution for FRP-concrete composite connections in comparison with the specimen with 16 mm studs.

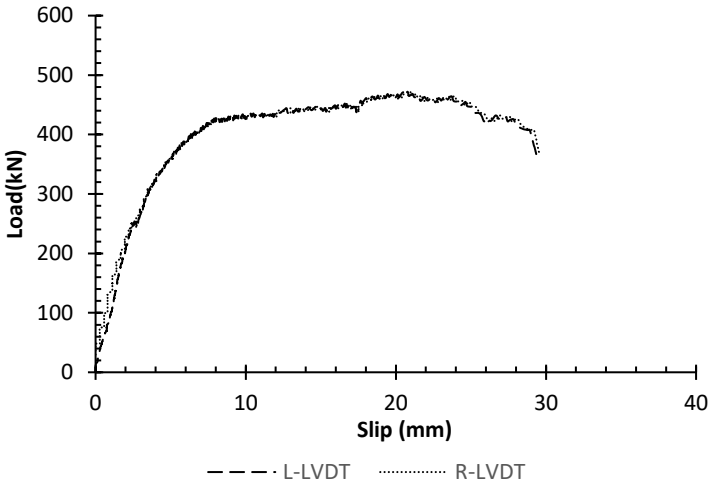

Fig. 8. Load-slip relationship (LVDTs).

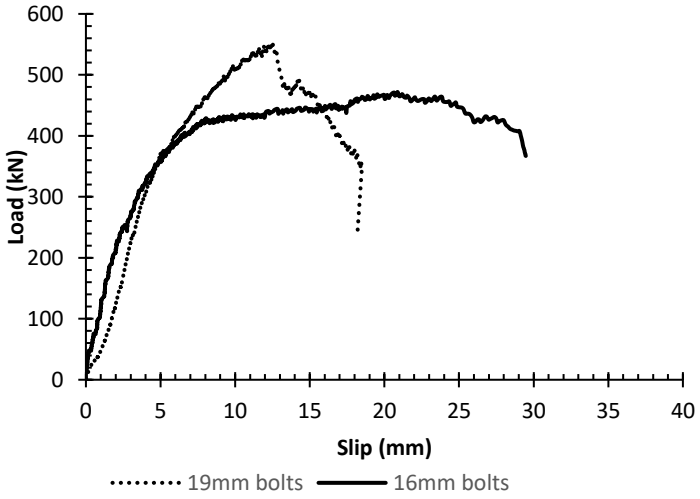

Fig. 9. Load-slip relationship – comparison of 19 mm stud and 16 mm stud.

6.3 Strain responses

Strain responses were recorded to evaluate the effect of the load on the stud-concrete and stud-FRP interactions. A knowledge of this is relevant in interpreting the overall performance and failure pattern exhibited in the composite connection. Phase 1 primarily captured only strain readings on FRP flanges at 100 mm distances above studs. Early observations in phase 1 informed modifications of 25 mm distance for strain readings on FRP flanges above stud and additional responses obtained from stud embedment in concrete.

6.3.1 Stud-strain response

This response forms the additional response obtained from phase 2 experimental testing in addition to the strain results from the FRP flanges. Figure 10 illustrates the strain response of the studs for specimen PO-12B-S4 at a position near the stud cap (Fig. 3b) was obtained, and the mean strain plotted. Strain readings became apparent on increase loading of 50 kN due to the position of the strain gauges on the studs. The gauges were positioned towards the stud cap to study the compression and anchor effect of the stud in concrete to mobilise resistance against the shear loading. The negative strain results suggest a compression force on the strain gauges rather than tension due to the compressive action of the concrete. The strain curve produces a linear progression transitioning into a nonlinear curve up unto failure. The nonlinear strain curve increases non-proportionally to increase loading, depicting increase resistance by the stud until failure. The strain measurements obtained are far lower in comparison to that obtained in FRP strain responses. At a maximum strain of about 1000 micro-strain on the stud, the FRP strain response transitions into the non-linear zone suggesting higher bearing interactions between the stud and the FRP flange.

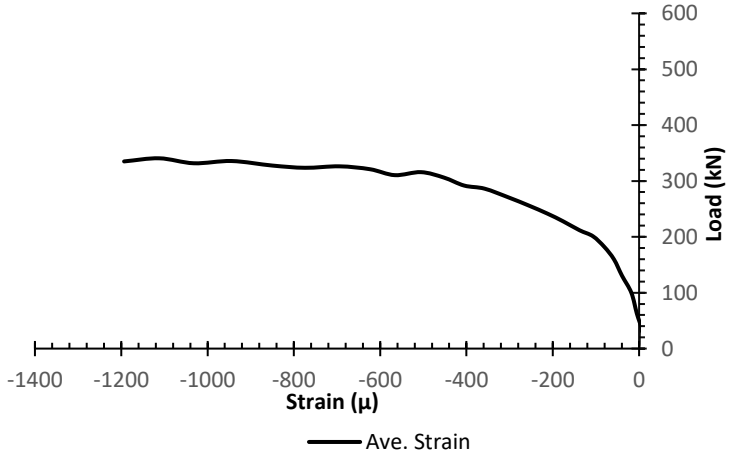

Fig. 10. Load-strain plot (stud strains).

The load-strain plot for the average strain at the position near the concrete/flange interface (Fig. 3a) is shown in Fig. 11. It clearly shows the average behaviour of the connection at the concrete-flange interface. The stud is under a tensile force that enhances the ductility of the connection. The steep profiles of the curve may suggest the sudden increases in loading due to the delamination failures of the FRP flange fibres also reaffirming a combined failure mode of stud deformation and bearing failures. However, at the ultimate load, another steep profile may conclude that the FRP flange plate forms the dominant failure mode of the connection.

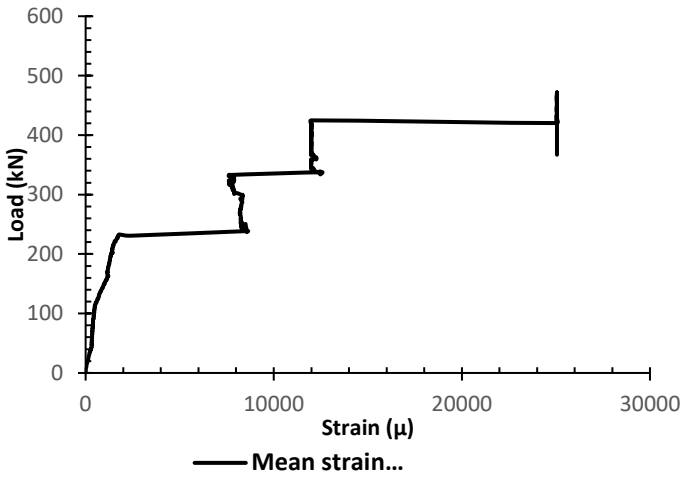

Fig. 11. Stud average strain plot – 16 mm studs.

6.3.2 Strain effect on FRP plates

The strain gauging for phase 1 included transverse and longitudinal gauges on the web and flanges of the FRP. However, strain readings from the transverse gauges were ignored, since the strain recordings were too insignificant compared to the longitudinal strains. The most significant readings obtained on the flanges are reported here for analysis. The above observation and analysis informed the decision to omit web gauging and transverse gauging in phase 2. A detailed analysis was obtained from phase 2 testing with a reduction in the measured distance for the position of strain gauge above the stud clearance holes on the GFRP flanges. The measured distance was reduced to 25mm, as stated in section 5.3. Results for strain responses from Specimen PO-12B-S5 is presented in Fig.12. The gauges were identified on the Right-hand side (RS) and Left-hand side (LS) of the slab and denoted as BL, BR, TL and TR for the bottom left, bottom right, top left and top right respectively. This was generally represented as RS-BL, LS-TR denoting right-hand side – bottom left clearance hole, left-hand side – top right, respectively as the case may be.

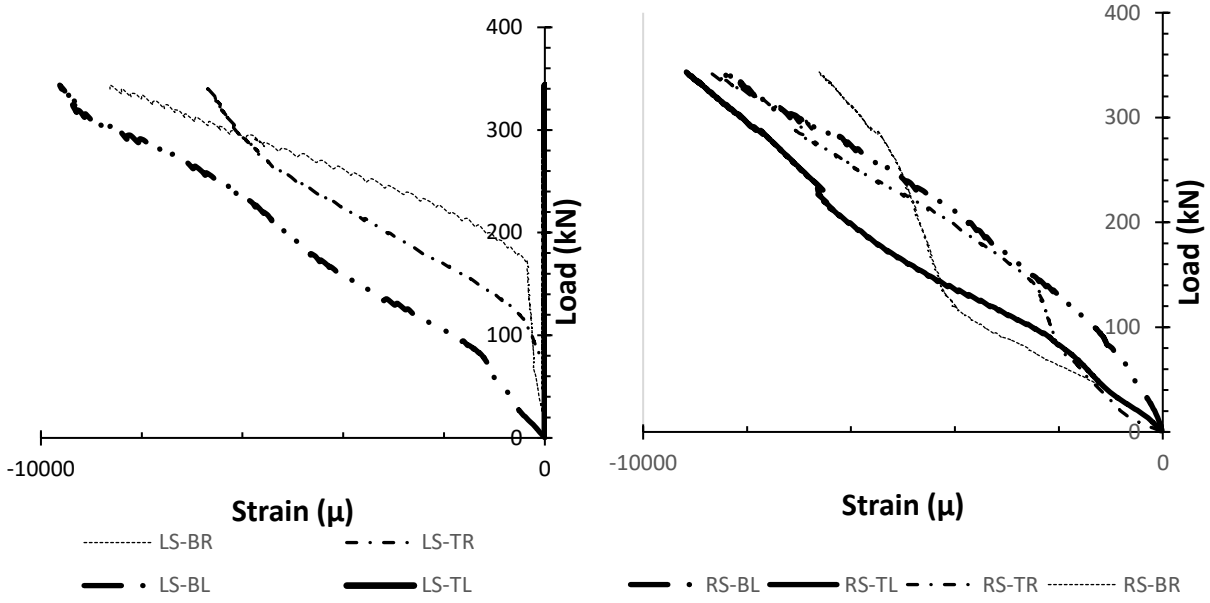

Fig. 12. FRP Strain response for specimen PO-12B-S5.

The load-strain plots obtained showed negative reading depicting compression of FRP fibres due to the load resistance on the bearing surface of the clearance holes by the shear stud. The stud provides a boundary resistance against the compressive load on the fibres. The strain readings, therefore, reflect the effect of the compressive forces on the fibres around the stud hole and the plotted lines are wavy on the graph indicating de-bonding of the material fibres from the matrix. The early linearity of the plot for clearance holes around the stud indicates the proportional response of load against strain during which the stud slips into bearing. After that, as the load increases, resistance increases propagating failure on the fibres of the FRP flange. The failure propagation on the fibre intensifies with a nonlinear curve represented on the graph until delamination becomes visible with the fibres on increasing load. The nonlinear curve continues to final failure, where further loading is not admissible. The final failure is represented on the graph at the peak of the plot in which case the fibres have been delaminated. The strain response of the various studs will differ, as seen in the plots in Fig. 12 because of the non-homogeneity of the FRP material.

The strain plot for the right-hand side slab showed higher strain readings at early loading in comparison to the left-hand side. This may be attributed to the difference in homogeneity between both flanges and a nonconsistency in the concrete mix between the slabs. However, this could be due to the load distribution on the studs either caused by the difference in concrete resistances allowing for the early mobilisation of strength in the studs located on the left-hand side slab. This is reflected in the difference between average strains on the left-hand side against that on the right-hand side

shown in Fig. 12. Figure 16(a) is an output by Nguyen [15] and illustrates the total average strain of all studs to the average strain at a distance 25 mm above the clearance holes. Nguyen [15] observed higher strains obtained at 25 mm position above the stud holes while lower strains were obtained at 50 mm above the holes and insignificant strain readings were taken at 25 mm beneath the bolt holes. The resulting strain at 25 mm above stud hole is compared against the equivalent strain data reported by Nguyen [15] at a similar position. The strain response reported by the same author was higher following the type of FRP material used, the size of the shear stud and concrete compressive strengths. The FRP material adopted was a hybrid polymer composed of carbon fibre for improved strength along with the ultra-high performance fibre reinforced concrete (UHPFRC) connected using 16 mm high strength steel stud. The strength enhancement of the connection resulted in a likely higher strain response around the stud holes when compared to the performance of GFRP- normal weight concrete composite using 12 mm steel studs. The negative curve pattern provided by both graphs implies a systematic response of the FRP material to shear loading, in this case, provides consistency to validate the hypothesis that the FRP flange property influences the shear behaviour of FRP-Concrete composites.

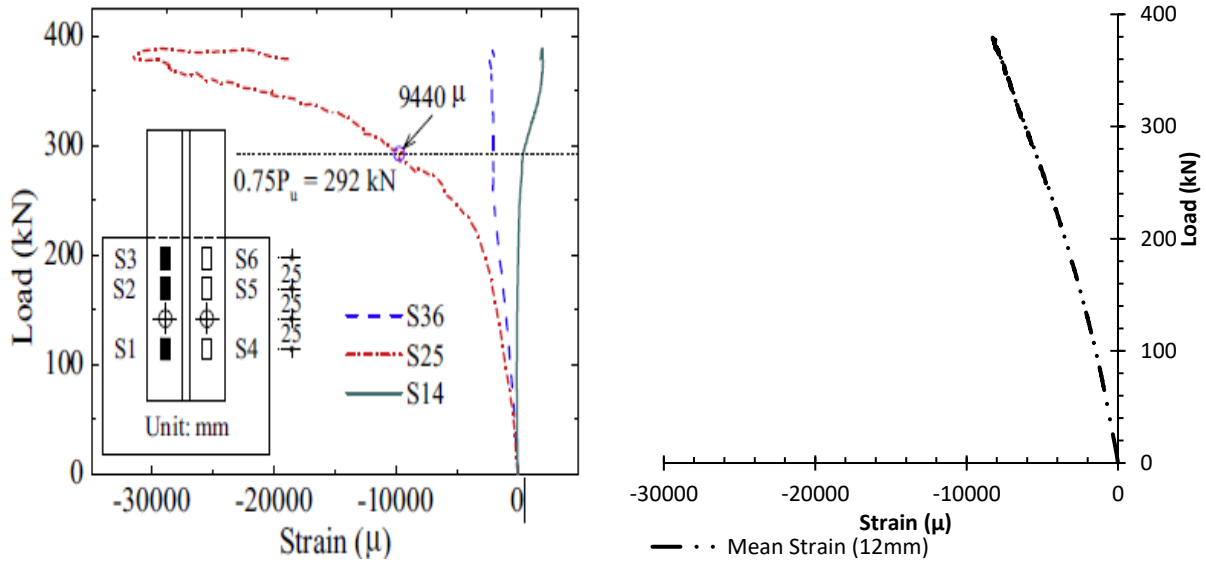

Fig. 13. FRP mean strain response - (a) Nguyen's [13] plot (b) current study.

6.4 Shear strength

Discussions on Sections 6.4 and 6.5 will be limited to specimens PO-12B-S4 and PO-12B-S5 of similar configuration to address the influence of stud size on shear capacity, ductility and stiffness. Experimental results show an increase in shear capacity following increase stud sizes. This indicates that the shear stud size influences the shear capacity of the connection; therefore, larger sizes, with respect to the stud shank diameter of studs will typically resist higher shear

loads. This forms a common composite behaviour for all types of composite connections, including FRP-concrete. However, there is an inconsistent shear value between specimens PO-12B-S4 and PO-12B-S5, with 12 mm shear stud, which may be due to the uneven distribution of concrete within the slab also suggesting the concrete curing process as an influence on composite behaviour. The shear strength of the connection will be derived from a critical value due to concrete failure or stud fracture (where the concrete has sufficient strength to enhance the mobilization of stud capacity, Dai *et al*. [19] for steel-concrete connection whereas, the critical value for shear resistance in an FRP-concrete may be assumed from a dominant bearing failure due to failure mode observed. At ultimate loading, the connection may have failed already due to the brittle nature of the FRP material. This clearly shows the influence of FRP mechanical properties in determining the shear resistance of FRP-concrete connections. Therefore, for an FRP material with higher strength properties, there will be a direct increase in shear capacity. The embedment depth of 100 mm was adopted to ensure an increase in shear capacity, as results are comparable to that reported by Nguyen [15], which showed that high embedment depths up to 50 mm enhanced shear capacity when compared to lower depths of 35 mm.

Table 4.

Theoretical comparison to experimental results (double row or eight bolt configurations).

Specimen ID	Experimental Strength per stud, P_{Exp} (kN)	Theoretical Strength per stud, P_{EC4} (kN)	Theoretical Strength per Stud, P_{OJ} (kN)	P_{Exp}/ P_{EC4}	P_{Exp}/ P_{OJ}
PO-12B-S4	41.63	34.04	29.56	1.22	1.41
PO-12B-S5	48.13	33.68	29.34	1.42	1.64
PO-16B-S6	53.84	56.61	50.05	0.95	1.08
PO-19B-S7	69.0	92.10	98.43	0.75	0.70

In Table 4, the theoretical predictions, according to Eqs. (1), (2) and (3) are compared against experimental results. Theoretical predictions for 12 mm stud are between 22 - 42% lower than the experimental result according to Eq. (2) of EC4 which provided the smaller value compared to Eq. (1). Using Eq. (3), according to [17] predicted between 41 – 64% lower values for shear strength against experimental results. Theoretical predictions for 16 mm bolt provided the closest of 5% higher value and an 8% lower value against experimental result for Eqs. (2) and (3), respectively. Lower values of 25% and 30% are predicted according to Eqs. (1) and (3) for 19 mm bolts. The consistent higher variability in results according to Eq. (3) is mostly due to the boundary conditions provided by the equation in which the girder influence is nullified and assumed rigid. This consideration does not, however, reflect the failure behaviour of our specimens and therefore suggest a stud fracture and concrete pull-out failure. The Eurocode 4 [1] predictions were closer to experimental results, which can be attributed to Eq. (2). It suggests a greater influence of concrete properties towards failure. This was observed in Fig. 9 where the strain on the stud increased due to compression forces toward the stud cap. This behaviour

suggested cracking failure in the concrete area around the stud cap and may be attributed for the proximity in prediction. The 19 mm studs were observed to be more rigid during testing and provided little or no deformation with the dominant failure seen to be bearing and tensile tear out. The non-conformity of the equation obtained from [1] towards the present study suggest the consideration of Nguyen's [15] modified equation for strength prediction. Stud sizes of 12 mm and 16 mm showed higher levels of disparity from about 22% to 42% confirming the insufficiency of the equation to be adapted towards FRP-concrete composites. Equation (4) as proposed by Nguyen [15] cannot be applied due to the unavailability of determined material properties of the GFRP profiles used in the study.

6.4.1 Steel-concrete Comparison

The obtained experimental test results on shear capacity from this study can be compared to results of steel-concrete push-outs reported in the literature. However, differences in shear capacity between results of this study and that reported by researchers in Table 5 may be further elaborated following the variations in the test conditions such as variations in concrete geometry, concrete properties, stud strength, test modifications and steel flanges. GFRP-concrete composites significantly provide a comparative performance with shear capacities of about 40-50 % that of steel-concrete counterparts.

Table 5.

Shear strength per stud comparison.

Stud Dia. (mm)	GFRP-concrete push-outs (kN)	Steel-concrete push-outs (kN)					
	Exp. test results	Nguyen *et al.* [15]	Ollgaard *et al.* [9]	Prakash *et al.* [14]	Odenbreit & Nellinger [12]	An and Cederwall [8]	Rehman *et al.* [17]
16	54	103	89	-	-	-	80
19	69	-	137	-	52	120	-
20	-	-	-	132	-	-	66

6.5 Shear stiffness and ductility

The shear stiffness of the connection between Specimen PO-12B-S4 and PO-12B-S5 shows a 35% difference in stiffness with specimen PO-12B-S5 having higher stiffness. This may be due to an initial slip during loading on specimen one owing to the bearing of the stud against the clearance hole on the FRP flange. This early slip caused a significant

difference in stiffness and can be attributed to a difference in torque applied to the stud. Specimen 5 provides a closer stiffness to specimen 6 with a difference of 14% lower stiffness to specimen 6 of 110 kN/mm stiffness as both curve profiles are not smooth, showing a wavy outlook. However, this clearly shows that if concrete compressive strength is high with consistent curing, the stud stiffness for a 12 mm and 16 mm stud is almost insignificantly similar. Stud stiffness may be mobilised from proper concrete curing with high compressive strength. Specimen PO-SG-S2, phase I exhibited a significant shear stiffness (of about 117% and 39% for specimen PO-SG-S1 and PO-SG-S2, respectively) due to observed load redistribution among the studs during experimental testing. At peak loads, an average slip up to 8 mm can be achieved with 12 mm and 16 mm studs, which satisfy the ductility requirement specified in [1]. The measured longitudinal depth of 4.5 mm for bearing failure shows the contribution of the FRP flange delamination in forming a pseudo-ductile slip, which clearly distinguishes the ductility of GFRP-concrete from the typical ductile behaviour for a steel-concrete composite.

7 Concluding remarks

The study presents the results of six push-out test performed within two phases, I and II of an experimental investigation on a GFRP-concrete composite connection. The test was performed on a characterised normal density concrete connection with GFRP to study the mode of failure, shear capacity and ductility properties of such a connection. The load-slip curves were plotted as well as the strain responses of both studs and FRP flange within the clearance zone for knowledge. The following concluding remarks are outlined:

- The shear capacity of a novel GFRP-concrete composite connection can mobilize up to 40-50 % shear resistances of the shear capacity of steel-concrete counterparts. GFRP-concrete composites can attain shear resistances of 54 kN per stud for stud sizes of 16 mm and 48 kN per stud for stud sizes of 12 mm. The applicability of higher shear stud sizes to attain higher resistances in steel-concrete composites is also valid for FRP-concrete composites. However, the intensity of bearing failure increases with increase in stud size, thereby compromising the ductility of connection.
- Using studs of diameter 19 mm caused significant fibre failure across the clearance hole in a transverse propagation. Therefore, it may be safe to adopt the 16 mm as a higher boundary for stud size.
- Flange bearing failures dominantly characterised the shear deformation failures of the push-out tests. This type of failure is capable of compromising the ductility of connection and therefore becomes significantly detrimental

to design. The critical load for a safe design becomes significantly low, assuming this load is defined as the load capable of propagating failure on the GFRP flange during loading.

- The analytical equations available in Eurocode 4 [1] does sufficiently predict the shear resistances and failure behaviour for an FRP-concrete composite connection. The prediction from [1] becomes too conservative and depicts concrete failure as against bearing failure. Therefore, the adoption of the proposed modified equation by Nguyen [15] is recommended for further investigation to proffer safe design guidelines.
- The degree of concrete compaction during curing is essential for proper distribution of aggregate around the bolt area for mobilisation of concrete strength and enhancement of stud stiffness.

Acknowledgements

The authors are particularly thankful to the technicians at the School of Energy, Construction and Environment, Coventry University, for their assistance in the fabrication of the test specimens.

References

[1] BS EN 1994-1-1: Design of Composite Steel and Concrete Structures. London: British Standards Institution; 2004.

[2] Neagoe C., Gil L. and Pérez, M. Experimental study of GFRP-concrete hybrid beams with a low degree of shear connection. Construction and Building Materials, 2015; 101, pp.141-151.

[3] Nguyen, H. and Kim, S. Finite element modelling of push-out tests for large stud shear connectors. Journal of Constructional Steel Research, 2009, 65(10-11), pp 1909-1920.

[4] Molkens, T., Dobric, J. and Rossi, B. Shear resistance of headed shear studs welded on welded plates in composite floors. Engineering Structures, 2019; Volume 197, pp 1-16

[5] Jin, D., Yang, Z., Xuhong, Z., Fengjiang Q., Xi P. Push-out test of large perfobond connectors in steel-concrete joints of hybrid bridges. Journal of Constructional Steel Research, 2018; 150, pp 415-429.

[6] Yang, F., Yuqing, L., Zhibo, J., and Haohui X. Shear performance of a novel demountable steel-concrete stud connector under static push-out tests. Engineering Structures, 2018; 160, pp 133-146.

[7] Emad, H., Shahrizan, B., Wan H., Badaruzzaman, W., Ahmed W. Push-out test on the web opening shear connector for a slim-floor steel beam: Experimental and analytical study. Engineering Structures, 2018; 163, pp 137-152.

[8] An, L., and Cederwall, L. Push-out tests on studs in high strength and normal strength concrete. Journal of Constructional Steel Research, 1996; 36, No. 1, pp 15-29.

[9] Ollgaard, J., Slutter, R., and Fisher, J. Shear strength of stud connectors in lightweight and normal-weight concrete. AISC Engineering Journal, 1971; pp 55-64.

[10] Kim, J., Kwark, J., Joh, C., Yoo, S. and Lee, K. Headed Stud Shear Connector for thin Ultrahigh-Performance Concrete Bridge Deck. Journal of Constructional Steel Research, 2015; Volume 108, pp 23 – 30.

[11] Hicks, S.J. and Smith, A.L. Stud shear connectors in composite beams that support slabs with profiled steel sheeting. Structural Engineering International: Journal of the International Association for Bridge and Structural Engineering (LABSE), 2014; 24 (2), pp 246-253.

[12] Odenbreit, C. and Nellinger, S. Mechanical model to predict the resistance of the shear connection in composite beams with deep steel decking. Steel Construction, 2017; 10 (3), pp 248-253.

[13] Gai, X., Darby, A., Ibell, T. and Evernden, M. Experimental investigation into a ductile FRP stay-in-place formwork system for concrete slabs. Construction and Building Materials, 2013; Volume 49, pp 1013 – 1023.

[14] Prakash, A., Anandavalli, N., Madheswaran, C. and Lakshmanan, N. Modified push-out tests for determining shear strength and stiffness of HSS stud connector: Experimental study. International Journal of Composite Materials, 2012; 2(3), pp 22-31.

[15] Nguyen, H., Mutsuyoshi, H., and Zatar, W. Push-out tests for shear connections between UHPFRC slabs and FRP girder. Composite Structures, 2014; 118 (1), pp 528-547.

[16] Correia J., Branco J., Ferreira J., (2005), "Structural behaviour of GFRP-concrete hybrid beams. Composites in Construction, 2005, 3rd International Conference, Lyon, France.

[17] Oehlers, D. J. and Johnson, R. P. The strength of stud shear connections in composite beams. Structural Engineer; 1987; 6(2), pp 44-48.

[18] Mottram, J. T. Determination of pin-bearing strength for the design of bolted connections with standard pultruded profiles. 4th International Conference on Advanced Composites in Construction, 2009, Net Composites Ltd, Chesterfield, pp 483-495.

[19] Dai, X., Lam, D. and Saveri, E. Effect of concrete strength and stud collar size to a shear capacity of demountable shear connectors. Journal of Structural Engineering, 2015; 141 (11), 04015025.

[20] Rehman, N., Lam, D., Dai, X. and Ashour, A. Experimental study on demountable shear connectors in composite slabs with profiled decking, Journal of Constructional Steel Research, 2016; 122, pp 178-189.